

Mitral Regurgitation Recognition based on Unsupervised Out-of-Distribution Detection with Residual Diffusion Amplification

Zhe Liu^{1,2*}, Xiliang Zhu^{1,2*}, Tong Han^{1,2*}, Yuhao Huang^{1,2}, Jian Wang³,
Lian Liu^{1,2,4}, Fang Wang⁵, Dong Ni^{1,2}, Zhongshan Gou⁵(✉), and
Xin Yang^{1,2}(✉)

¹National-Regional Key Technology Engineering Laboratory for Medical Ultrasound, School of Biomedical Engineering, Medical School, Shenzhen University, China

²Medical Ultrasound Image Computing (MUSIC) Lab, Shenzhen University, China

³Key Laboratory for Bio-Electromagnetic Environment and Advanced Medical Theranostics, School of Biomedical Engineering and Informatics, Nanjing Medical University, China

⁴Shenzhen RayShape Medical Technology Co., Ltd, China

⁵Center for Cardiovascular Disease, The Affiliated Suzhou Hospital of Nanjing Medical University, China

Abstract. Mitral regurgitation (MR) is a serious heart valve disease. Early and accurate diagnosis of MR via ultrasound video is critical for timely clinical decision-making and surgical intervention. However, manual MR diagnosis heavily relies on the operator’s experience, which may cause misdiagnosis and inter-observer variability. Since MR data is limited and has large intra-class variability, we propose an unsupervised out-of-distribution (OOD) detection method to identify MR rather than building a deep classifier. To our knowledge, we are the first to explore OOD in MR ultrasound videos. Our method consists of a feature extractor, a feature reconstruction model, and a residual accumulation amplification algorithm. The feature extractor obtains features from the video clips and feeds them into the feature reconstruction model to restore the original features. The residual accumulation amplification algorithm then iteratively performs noise feature reconstruction, amplifying the reconstructed error of OOD features. This algorithm is straightforward yet efficient and can seamlessly integrate as a plug-and-play component in reconstruction-based OOD detection methods. We validated the proposed method on a large ultrasound dataset containing 893 non-MR and 267 MR videos. Experimental results show that our OOD detection method can effectively identify MR samples.

1 Introduction

Mitral regurgitation (MR) is a significant heart valve disorder that becomes more common with advancing age. It may cause heart size changes, decreased

* Zhe Liu, Xiliang Zhu and Tong Han contribute equally to this work.

Corresponding authors’ email: gzhongshan1986@163.com and xinyang@szu.edu.cn

cardiac function, and even life-threatening consequences [5]. Early detection and accurate assessment of MR enables timely intervention, holding vital clinical significance. Color Doppler echocardiography is the primary tool to diagnose MR, enabling visualization of blood flow direction and velocity within the heart that is not visible in standard B-mode ultrasound [22]. However, manual assessment is subjective and easily affected by experts’ experience, potentially leading to diagnostic errors and observer inconsistency. Figure 1 shows the challenges in MR recognition, where similar features appear in both negative and positive cases.

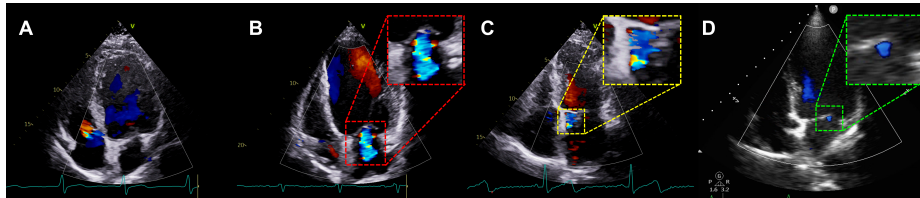


Fig. 1. The challenges encountered in OOD detection for our task. **A)** Negative sample, **B)** Positive sample, **C)** Negative sample with artifacts similar to regurgitation, **D)** Positive samples of reflux bundles resembling artifacts.

Deep learning techniques can potentially address the above problems, e.g., by training a classifier to recognize MR. However, the limited availability of MR data and its significant intra-class variability compared to normal data can constrain the performance of binary classifier [12]. For example, the imbalanced data distribution caused by the lack of MR data can severely affect the performance of supervised methods [8, 13, 21]. Recently, there have been significant advancements in out-of-distribution (OOD) detection, opening up new possibilities for MR recognition. The goal of OOD detection is to identify samples that are inconsistent with the distribution of in-distribution (ID) data (i.e., training data) [20]. It is noted that in MR recognition, numerous normal samples with similar features are regarded as ID data, and minimal but diverse MR cases are considered OOD data. Although promising, we found that studies applying OOD detection to MR recognition have not yet been reported.

Applying existing OOD research to MR recognition without modification may face several challenges. Unsupervised OOD detection methods for videos showed great potential, and they mainly included two main streams: frame prediction and generation techniques. Among frame prediction methods, those using optical flow maps [1, 4] and long sequences of observations [2, 18] were deemed inadequate for MR ultrasound videos due to noise, artifacts, and the cardiac cycle’s motion pattern. Besides, generation-based approaches may encounter information bottlenecks caused by discrepancies between potential input dimensions and the dimensions reconstructed by the model [6, 15]. The diffusion model solely employed the mean and standard deviation for denoising the reconstructed im-

age, thereby mitigating the bottleneck issue mentioned previously to ensure the reconstruction of echocardiographic videos [6, 13, 19].

In this study, we propose a diffusion-based unsupervised OOD detection method for recognizing MR from echocardiography videos. Specifically, we first employ pre-trained models as feature extractors to extract features from video clips. Second, we train a diffusion model for feature-level reconstruction. Last, we design a residual accumulation amplification algorithm during the testing phase. This algorithm iteratively performs noise feature selection and reconstruction, amplifying the reconstructed error of OOD features. We validate the proposed method on a large four-chamber cardiac (4CC) ultrasound video dataset containing 893 non-MR and 267 MR videos, and the experimental results show that the proposed method is effective. We believe we are the first to explore OOD detection in MR recognition with echocardiography videos.

2 Methodology

As shown in Figure 2, our method consists of a feature extractor, a feature reconstruction model, and a residual accumulation amplification algorithm. The feature extractor catches features from video clips and inputs them into the reconstruction model to rebuild the features. Then, during testing, under the proposed residual accumulation amplification algorithm, the OOD data can gradually be more distinguishable from the ID data.

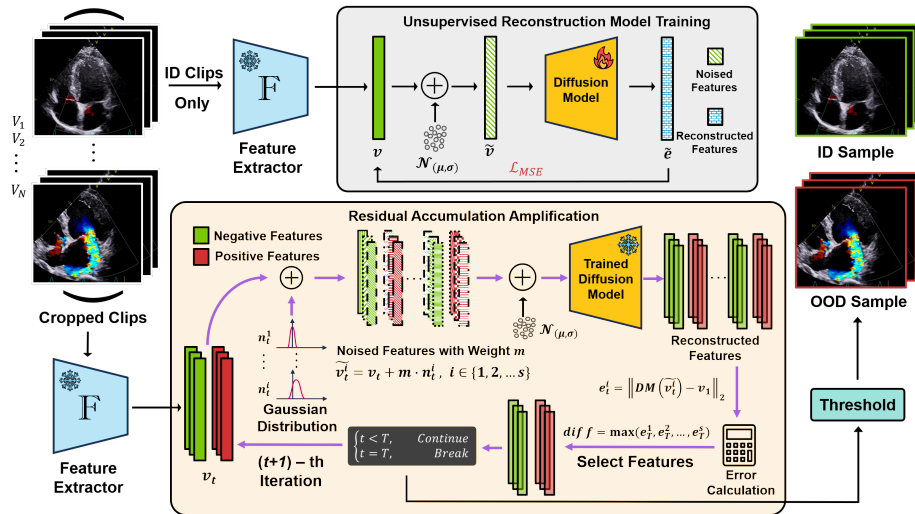


Fig. 2. Overview of our proposed method.

2.1 Representative Feature Extractor

The feature extractor aims to capture essential knowledge from video clips. Let $V \in R^{k \times 3 \times h \times w}$ denote a video clip consisting of k consecutive RGB images with a resolution of $h \times w$ pixels, the feature $v \in R^l$ is obtained by feeding V into the feature extractor $f(\cdot)$. The architecture of the feature extractor is flexible and can be convolutional neural networks, long short-term memory, visual transformers, and their hybrids. Here, we tried several models, including 3D-ResNet18 [7], 3D-ResNet101 [7], Video MAE [16], and X-CLIP [14]. These models were pretrained on Kinetics-400 [3], a large-scale dataset containing more than 160,000 videos with 400 categories. We froze the models’ weights without any fine-tuning.

2.2 Feature Reconstruction Model

The diffusion model gains the capability to generate diverse samples by disrupting training samples with noise and learning the reverse process. For a given video clip V , features are obtained by $v = f(V)$. The process of feature disruption can be formulated as a progressive addition of Gaussian noise (standard deviation: σ) to the input data v_T obtained by sampling from a data distribution $p_{data}(v)$ with standard deviation σ_{data} . After adding noise, the data distribution could be represented as $p(v; \sigma)$ and $p(v; \sigma_{min}) \approx p_{data}(v)$ ideally. If $\sigma_{max} \gg \sigma_{data}$, the $p(v; \sigma)$ becomes isotropic Gaussian and allows to sample a data $v_0 \sim \mathcal{N}(0, \sigma_{max}I)$. The reversed process of diffusion model can be formulated as v_0 being gradually denoised with noise levels $\sigma_0 = \sigma_{max} > \sigma_1 > \dots > \sigma_T = 0$ into new samples, until it becomes a data with data distribution of $p_{data}(v)$.

In detail, we follow the diffusion model in [10], treating $s_\theta(\tilde{v}, \sigma)$ as a denoising function that directly estimates denoised samples with target function \mathcal{L} :

$$\mathcal{L} = E_{v \sim p_{data}} E_{\epsilon \sim \mathcal{N}(0, \sigma I)} \|s_\theta(v + \epsilon; \sigma) - v\|_2. \quad (1)$$

Besides, in [10], researchers untangled the design choices of previous diffusion models and offered a framework where each component (Sampling, Network and preconditioning, Training) can be adjusted independently. Therefore, in our study, the denoising function $s_\theta(\cdot)$ is formulated as follows:

$$s_\theta(v; \sigma) = c_{skip}(\sigma)v + c_{out}(\sigma) * F_\theta(c_{in}(\sigma)v; c_{noise}(\sigma)), \quad (2)$$

where $F_\theta(\cdot)$ is a multi-layer perceptron (MLP) with an encoder-decoder structure. $c_{skip}(\cdot)$ modulates the skip connection. $c_{out}(\cdot)$ and $c_{in}(\cdot)$ scale magnitudes of the noise variance. $c_{noise}(\cdot)$ scales θ to a suitable value for the input of $F_\theta(\cdot)$.

The reverse process of disrupting samples in the feature reconstruction of video clips can be formulated as:

$$\tilde{v}_t = \tilde{v}_{t-1} + \frac{\varepsilon}{2}s_\theta(\tilde{v}_{t-1}, \sigma) + \sqrt{\varepsilon}z_t, \quad (3)$$

where $\varepsilon > 0$ is a predefined step size and $z_t \sim \mathcal{N}(0, I)$ is random term. With certain constraints, reversing multiple times at very small step sizes results in the final generated sample obeying the distribution $p_{data}(v)$.

The diffusion process is governed by multiple hyperparameters, with our main focus being the exploration of the effect of noise distribution on model performance. For fair comparisons, we follow [17] to determine other settings, including model structure, learning rate scheduler, etc. The diffusion model is central to the OOD detection model, used to recover the samples after being corrupted with Gaussian noise during the testing phase. The OOD information is derived by evaluating the discrepancy between samples before and after restoration.

2.3 Residual Accumulation Amplification

Inspired by the genetic accumulation of mutated genes with inheritance in genetics [9], we designed a residual accumulation amplification algorithm used in the testing stage. The core of the algorithm involves selecting MR recognition-related features and amplifying the reconstruction error via multiple iterations of noise feature reconstruction to enhance the distinction between OOD and ID data. In each iteration, we first randomly sample s Gaussian noises from the normal distribution $\mathcal{N}(\mu, \sigma)$, and then add them to the anchor feature to randomly destroy features that represent different information. The formula is as follows:

$$\tilde{v}_t^i = v_t + m \cdot n_t^i, \quad i \in \{1, 2, \dots, s\}, \quad (4)$$

where n^i denotes the sampled Gaussian noise and m denotes the weight of noise. v and \tilde{v}^i represent the anchor and noise features, respectively. t is the current iteration number. In the first iteration, the anchor feature (v_1) is extracted from the video clips using the feature extractor. Those noise features are fed into the reconstruction model, and the reconstructed error is calculated as follows:

$$e_t^i = \|DM(\tilde{v}_t^i) - v_1\|_2, \quad i \in \{1, 2, \dots, s\}, \quad (5)$$

where $DM(\cdot)$ denotes the reconstruction model and e_t^i denotes the reconstructed error in the t -th iteration. $\|\cdot\|_2$ represents the L_2 norm.

As shown in Figure 3 (D), OOD data is more sensitive to reconstruction, and the difference between the reconstruction error of ID and OOD data will increase after multiple reconstructions. Therefore, we continue to add Gaussian noise to the current noise features for the next reconstruction. The noise feature corresponding to the maximum error is selected as the anchor feature in the next iteration. We believe that the larger error arises from the destruction of features unrelated to MR recognition. As these irrelevant features are eliminated after multiple iterative selections, the remaining features that are more related to MR recognition can enhance the detection efficacy:

$$v_{t+1} = \arg \max_{\tilde{v}_t} (e_t). \quad (6)$$

The reconstruction error continues to be amplified until the stopping condition is reached, that is, $t = T$. The maximum error in the last iteration is regarded as the difficulty of feature reconstruction: $diff = \max(e_T^1, e_T^2, \dots, e_T^s)$. The sample is classified according to a data-driven threshold ($thre$), defined as $thre = \mu_{diff} + 0.001\sigma_{diff}$, where μ_{diff} and σ_{diff} are the mean and standard deviation of the difficulty of feature reconstruction in the validation set.

Table 1. Comparison of our method with 3D-ResNet50 and unsupervised methods.

Supervised Methods	F1-score	Recall	Precision	Specificity	Accuracy
3D-ResNet50(N=240) [7]	0.0246	0.0128	0.3333	0.9845	0.6167
3D-ResNet50(N=360) [7]	0.7338	0.8213	0.6632	0.7461	0.7746
3D-ResNet50(N=480) [7]	0.7549	0.8255	0.6953	0.7798	0.7971
Unsupervised Methods	F1-score	Recall	Precision	Specificity	Accuracy
Diffusion + Star [17]	0.4921	0.5545	0.4423	0.5822	0.5719
Diffusion + Dyn [17]	0.4964	0.5446	0.4561	0.6118	0.5867
HF ² VAD [11]	0.4800	0.5347	0.4355	0.5858	0.5667
Ours	0.5545	0.5883	0.5244	0.6342	0.6156

3 Experimental Results

3.1 Dataset and Implementations

The 4CC ultrasound video dataset was collected, comprising 893 non-MR and 267 MR videos. Regions of interest were extracted from frames originally sized at 1016×708 and resized to 224×224 for further processing. Multiple non-overlapping video clips were sampled from each video, and each clip consists of 16 consecutive frames, resulting in 3480 clips. Those clips cropped from MR videos are designated as positive samples (i.e., OOD samples), while others are taken as negative samples (i.e., ID samples). The dataset was divided into a training set with 1506 ID clips, a validation set with 621 clips (372 ID/249 OOD), and a testing set with 1353 clips (801 ID/552 OOD).

We adopted log-normal sampling (mean: -0.05, var: 1.5) for noise generation. Training epoch is set to 100 with *batch size*=64, using the AdamW optimizer with *learning rate*=0.0002. We used five metrics for evaluation: F1-score, Recall, Precision, Specificity, and Accuracy. All experiments were conducted on the *PyTorch* 2.0.1 framework with NVIDIA Tesla A40 GPUs.

3.2 Performance Comparisons

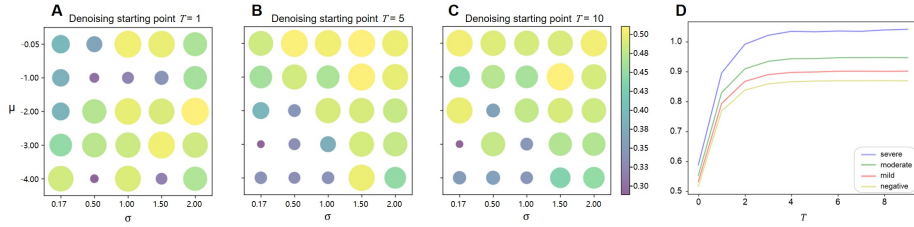
We compared our proposed method with a basic supervised classification method (3D-ResNet50) and other reconstruction-based unsupervised OOD detection methods under the same settings. In 3D-ResNet50, we gradually increased the number of OOD clips N in the training set. As shown in Table 1, the proposed method surpasses previous unsupervised methods and even surpasses 3D-ResNet50 with limited OOD data.

3.3 Comparison of Feature Extractor

We compared the MR recognition performance under different feature extractors. Thus, we used X-CLIP as the backbone in the following experiments for it achieved the best results in Table 2. The X-CLIP extractor with Transformer

Table 2. Performance comparison of OOD models with different feature extractors.

Model	F1-score	Recall	Precision	Specificity	Accuracy
3D-ResNet18 [7]	0.3193	0.255	0.4268	0.7653	0.5578
3D-ResNes101 [7]	0.3218	0.2459	0.4655	0.8065	0.5785
VideoMAE [16]	0.4124	0.4226	0.4028	0.5705	0.5104
X-CLIP [14]	0.5116	0.5228	0.5009	0.6429	0.5941

**Fig. 3.** (A-C) The effect of noise and the starting point of the reverse process. The larger the circle area, the greater the difference between the features. (D) Reconstruction difference among different subclasses of MR samples with feature amplification.

modules pretrained on a vast video dataset has a stronger capability to capture rich semantic information. This may be because text-video model fusion allows a more comprehensive understanding of complex features by capturing diverse aspects of the data. The performance gap between Convolution-based models and Transformer-based models can be attributed to the superior ability of Transformer with self-attention modules in learning long-range dependence features compared to convolutional modules. Particularly in video tasks with temporal information, Transformers exhibit advantages due to their enhanced capability to capture temporal dependencies and patterns.

3.4 Diffusion Model Analysis

We tend to find the optimal T and $\mathcal{N}(\mu, \sigma)$ to preserve sufficient structural information of the video clip while disrupting potential anomaly information. Then, higher reconstruction errors can be obtained to judge the associated video frames as abnormal. For Gaussian distributions $\mathcal{N}(\mu, \sigma)$, μ ranges from -0.05 to -4 and σ ranges from 0 to 2. Besides, the start points T of the reverse process are set to 1, 5 and 10. For each value of T , 25 different Gaussian noise samples can be produced, as shown in Figure 3 (A-C). It can be observed that $\mu = -0.05$, $\sigma = 1.5$ and $T = 5$ obtain the best score. Overall, increasing the T value while fixing μ and σ can improve the OOD detection results. σ is the primary determinant of the model. Specifically, the performance gap for changing the value of σ is 3% in the F1-score, with all other hyperparameters remaining constant.

Table 3. Performance Comparison with different parameters. Bold: the final model adopted in our work. The feature extractor is a pretrained X-CLIP.

T	s	m	F1-score	Recall	Precision	Specificity	Accuracy
1	1	0	0.5116	0.5228	0.5009	0.6429	0.5941
2	1	0	0.5081	0.5118	0.5045	0.6554	0.5970
3	1	0	0.5036	0.5064	0.5009	0.6542	0.5941
4	1	0	0.5041	0.5046	0.5036	0.6592	0.5963
5	1	0	0.5246	0.5337	0.5158	0.6567	0.6067
10	1	0	0.5132	0.5118	0.5147	0.6650	0.6022
5	3	1	0.5426	0.5683	0.5191	0.6392	0.6104
5	3	1.5	0.5530	0.5847	0.5245	0.6367	0.6156
5	3	1.6	0.5547	0.5865	0.5261	0.6380	0.6170
5	3	1.7	0.5547	0.5865	0.5261	0.6380	0.6170
5	3	1.8	0.5545	0.5883	0.5244	0.6342	0.6156
5	3	1.9	0.5515	0.5847	0.5220	0.6330	0.6133
5	3	2	0.5526	0.5883	0.5210	0.6292	0.6126

Table 4. OOD performance of the reconstruction model with different modules.

Model	F1-score	Recall	Precision	Specificity	Accuracy
Baseline	0.5116	0.5228	0.5009	0.6429	0.5941
Baseline+RA	0.5246	0.5337	0.5158	0.6567	0.6067
Baseline+RA+NS	0.5545	0.5883	0.5244	0.6342	0.6156

3.5 Residual Accumulation Amplification Analysis

Residual accumulation amplification consists of residual accumulation (RA) and noise sampling (NS). This section analyzes the impact of both components on MR recognition performance. For RA, the reconstruction is iterated T times (i.e., 1, 2, 3, 4, 5, and 10). Table 3 shows that when T is set to 5, the diffusion model achieves optimal detection results on all metrics, and $T=10$ causes a slight performance drop. For NS, we use the control variable method to assess how different parameters affect diffusion model performance. First, we set the noise sampling number $s=3$ as a trade-off for computational efficiency. Then we change the weight of noise m to analyze its impact. Results in Table 3 show that consistent optimal results across all metrics can not be obtained with a single set of parameters. But in general, the number of iterations $T=5$ can get good results easier. Finally, we choose the optimal hyperparameters ($m = 1.8$, $s = 3$, $T = 5$) to construct the OOD detection model. The impact of each module on model performance is shown in Table 4. RA improves the model performance by amplifying the difference between ID and OOD data reconstruction errors, which is consistent with Figure 3 (D). However, its impact is limited by irrelevant features in the extracted information. NS addresses this issue effectively,

significantly boosting performance by retaining MR recognition-relevant features through iterative selections.

4 Conclusion

We propose an innovative model tailored for recognizing MR echocardiographic videos using an unsupervised OOD detection approach. Our model exclusively leverages features extracted from ID samples by a fixed-weight feature extractor to train the diffusion model. Subsequently, by iteratively introducing disturbance, the model selects MR recognition-related features and amplifies the difference between reconstruction errors of OOD and ID data. Comprehensive experimentation conducted on MR datasets substantiates the efficacy of our proposed method. Future endeavors may explore expanding our approach to encompass multi-classification within the OOD samples.

Acknowledgement. This work was supported by the grant from National Natural Science Foundation of China (12326619, 62101343, 62171290), Science and Technology Planning Project of Guangdong Province (2023A0505020002), Shenzhen-Hong Kong Joint Research Program (SGDX20201103095613036) and Suzhou Gusu Health Talent Program (GSWS 2022071, GSWS 2022072).

Disclosure of Interests. The authors have no competing interests to declare that are relevant to the content of this article.

References

1. Baradaran, M., Bergevin, R.: Object class aware video anomaly detection through image translation. In: 2022 19th Conference on Robots and Vision (CRV). pp. 90–97. IEEE (2022)
2. Baradaran, M., Bergevin, R.: Future video prediction from a single frame for video anomaly detection. In: International Symposium on Visual Computing. pp. 472–486. Springer (2023)
3. Carreira, J., Zisserman, A.: Quo vadis, action recognition? a new model and the kinetics dataset. In: proceedings of the IEEE Conference on Computer Vision and Pattern Recognition. pp. 6299–6308 (2017)
4. Duman, E., Erdem, O.A.: Anomaly detection in videos using optical flow and convolutional autoencoder. *IEEE Access* **7**, 183914–183923 (2019)
5. El Sabbagh, A., Reddy, Y.N., Nishimura, R.A.: Mitral valve regurgitation in the contemporary era: insights into diagnosis, management, and future directions. *JACC: Cardiovascular Imaging* **11**(4), 628–643 (2018)
6. Graham, M.S., Pinaya, W.H., Tudosi, P.D., Nachev, P., Ourselin, S., Cardoso, J.: Denoising diffusion models for out-of-distribution detection. In: Proceedings of the IEEE/CVF Conference on Computer Vision and Pattern Recognition. pp. 2947–2956 (2023)
7. Hara, K., Kataoka, H., Satoh, Y.: Learning spatio-temporal features with 3d residual networks for action recognition. In: Proceedings of the IEEE international conference on computer vision workshops. pp. 3154–3160 (2017)

8. Hendrycks, D., Gimpel, K.: A baseline for detecting misclassified and out-of-distribution examples in neural networks. arXiv preprint arXiv:1610.02136 (2016)
9. Holland, J.H.: Adaptation in natural and artificial systems: an introductory analysis with applications to biology, control, and artificial intelligence. MIT press (1992)
10. Karras, T., Aittala, M., Aila, T., Laine, S.: Elucidating the design space of diffusion-based generative models. In: Advances in Neural Information Processing Systems. vol. 35, pp. 26565–26577. Springer (2022)
11. Liu, Z., Nie, Y., Long, C., Zhang, Q., Li, G.: A hybrid video anomaly detection framework via memory-augmented flow reconstruction and flow-guided frame prediction. In: Proceedings of the IEEE/CVF international conference on computer vision. pp. 13588–13597 (2021)
12. Lu, J.C., Sable, C., Ensing, G.J., Webb, C., Scheel, J., Aliku, T., Lwabi, P., Godown, J., Beaton, A.: Simplified rheumatic heart disease screening criteria for handheld echocardiography. *Journal of the American Society of Echocardiography* **28**(4), 463–469 (2015)
13. Mishra, D., Zhao, H., Saha, P., Papageorghiou, A.T., Noble, J.A.: Dual conditioned diffusion models for out-of-distribution detection: Application to fetal ultrasound videos. In: International Conference on Medical Image Computing and Computer-Assisted Intervention. pp. 216–226. Springer (2023)
14. Ni, B., Peng, H., Chen, M., Zhang, S., Meng, G., Fu, J., Xiang, S., Ling, H.: Expanding language-image pretrained models for general video recognition. In: European Conference on Computer Vision. pp. 1–18. Springer (2022)
15. Serrà, J., Álvarez, D., Gómez, V., Slizovskaia, O., Núñez, J.F., Luque, J.: Input complexity and out-of-distribution detection with likelihood-based generative models. arXiv preprint arXiv:1909.11480 (2019)
16. Tong, Z., Song, Y., Wang, J., Wang, L.: Videomae: Masked autoencoders are data-efficient learners for self-supervised video pre-training. *Advances in neural information processing systems* **35**, 10078–10093 (2022)
17. Tur, A.O., Dall’Asen, N., Beyan, C., Ricci, E.: Unsupervised video anomaly detection with diffusion models conditioned on compact motion representations. In: International Conference on Image Analysis and Processing. pp. 49–62. Springer (2023)
18. Wang, X., Che, Z., Jiang, B., Xiao, N., Yang, K., Tang, J., Ye, J., Wang, J., Qi, Q.: Robust unsupervised video anomaly detection by multipath frame prediction. *IEEE transactions on neural networks and learning systems* **33**(6), 2301–2312 (2021)
19. Wyatt, J., Leach, A., Schmon, S.M., Willcocks, C.G.: Anoddpn: Anomaly detection with denoising diffusion probabilistic models using simplex noise. In: Proceedings of the IEEE/CVF Conference on Computer Vision and Pattern Recognition. pp. 650–656 (2022)
20. Yang, J., Zhou, K., Li, Y., Liu, Z.: Generalized out-of-distribution detection: A survey. arXiv preprint arXiv:2110.11334 (2021)
21. Zhang, J., Inkawhich, N., Linderman, R., Chen, Y., Li, H.: Mixture outlier exposure: Towards out-of-distribution detection in fine-grained environments. In: Proceedings of the IEEE/CVF Winter Conference on Applications of Computer Vision. pp. 5531–5540 (2023)
22. Zoghbi, W.A., Enriquez-Sarano, M., Foster, E., Grayburn, P.A., Kraft, C.D., Levine, R.A., Nihoyannopoulos, P., Otto, C.M., Quinones, M.A., Rakowski, H.,

et al.: Recommendations for evaluation of the severity of native valvular regurgitation with two-dimensional and doppler echocardiography. *Journal of the American Society of Echocardiography* **16**(7), 777–802 (2003)